Pergamon

J. Mech. Phys. Solids, Vol. 43, No. 9, pp. 1349–1362, 1995
Elsevier Science Ltd
Printed in Great Britain

0022–5096(95)00050–X

AN ALGORITHM FOR COMPUTING THE EFFECTIVE LINEAR ELASTIC PROPERTIES OF HETEROGENEOUS MATERIALS: THREE-DIMENSIONAL RESULTS FOR COMPOSITES WITH EQUAL PHASE POISSON RATIOS

E. J. GARBOCZI

Building Materials Division, National Institute of Standards and Technology, Building 226, Room B350, Gaithersburg, MD 20899, U.S.A.

and

A. R. DAY

Marquette University, Department of Physics, Milwaukee. WI 53233, U.S.A.

(*Received* 3 *December* 1994; *in revised form* 13 *May* 1995)

ABSTRACT

An algorithm based on finite elements applied to digital images is described for computing the linear elastic properties of heterogeneous materials. As an example of the algorithm, and for their own intrinsic interest, the effective Poisson's ratios of two-phase random isotropic composites are investigated numerically and via effective medium theory, in two and three dimensions. For the specific case where both phases have the same Poisson's ratio ($\nu_1 = \nu_2$), it is found that there exists a critical value ν^*, such that when $\nu_1 = \nu_2 > \nu^*$, the composite Poisson's ratio ν always decreases and is bounded below by ν^* when the two phases are mixed. If $\nu_1 = \nu_2 < \nu^*$, the value of ν always increases and is bounded above by ν^* when the two phases are mixed. In d dimensions, the value of ν^* is predicted to be $1/(2d-1)$ using effective medium theory and scaling arguments. Numerical results are presented in two and three dimensions that support this picture, which is believed to be largely independent of microstructural details.

1. INTRODUCTION

In previous papers (Snyder *et al.*, 1992; Day *et al.*, 1992), an algorithm combining digital-image and spring network techniques was developed and applied to study the effective moduli of 2-D random isotropic composites. Three limitations were: (1) the digital resolution required to represent the desired microstructure; (2) the Poisson's ratios of each phase were required to be greater than or equal to 1/3; and (3) the geometry of the digital representation was hexagonal pixels arranged on a triangular lattice. The first limitation is of course inherent to any numerical digitization scheme, while the second and third limitations were a result of the spring lattice technique used.

The specific case of two-phase composites, where each phase had the same Poisson's ratio but different Young's modulus, was studied using the above algorithm (Snyder

et al., 1992). It was found numerically that when the phase Poisson's ratios, $\nu_1 = \nu_2$, were above a critical value $\nu^* = 1/3$, the composite or effective Poisson's ratio ν was always greater than 1/3 and less than $\nu_1 = \nu_2$. Effective medium theory (Thorpe and Sen, 1985) was shown to describe the results (Snyder *et al.*, 1992; Day *et al.*, 1992) rather accurately. The validated effective medium theory was then used to show that when $\nu_1 = \nu_2 < 1/3$, the value of ν was always less than 1/3 and greater than $\nu_1 = \nu_2$. When $\nu_1 = \nu_2 = 1/3$, $\nu = 1/3$ as well, within a few percent accuracy. The effective medium theory predicted that $\nu^* = 1/3$ exactly, with this value being a fixed point for any area fraction of the two phases.

These results were obtained for microstructures composed of circular inclusions of one phase distributed randomly in a matrix of the other phase, with either freely overlapping circles or hard circles that were not allowed to overlap.

In the present work, we describe an algorithm that can compute the effective moduli of a composite in 2-D or 3-D, for arbitrary values of Poisson's ratio and Young's modulus. It can also handle anisotropic elastic stiffness tensors, for any number of phases. The microstructure of the composite, as long as it can be adequately represented by an ordinary digital image, can be completely general. In particular, the composite microstructure is definitely not limited to the case usually considered in analytic treatment of composites, that of inclusions with a simple geometry randomly placed in a matrix. This algorithm was developed to operate on model and real 3-D digital images of materials with complex microstructures, as part of a general program studying the various physical properties of such materials (Garboczi and Bentz, 1993). This program is being carried out in order to develop quantitative theoretical microstructure–property relationships in heterogeneous materials complex enough to require such models, like cement-based materials (Garboczi and Bentz, 1993) and sintered ceramic materials (Pimienta *et al.*, 1992).

To illustrate the operation of the elastic algorithm, we use a general non-particle-based microstructure introduced recently (Schwartz *et al.*, 1991) to study the composite Poisson's ratio for the case of equal phase Poisson's ratios in 3-D, and in 2-D for cases that were inaccessible to our previous algorithm.

2. ALGORITHMS

The problem of determining the effective linear elastic properties of random, multiphase materials is an old, difficult and important problem (Watt *et al.*, 1991; Hashin, 1983; Torquato, 1991). Much can be done analytically in the case where the composite is made up of inclusions having simple geometries that are randomly or regularly embedded in a matrix. However, many materials, like polycrystalline ceramics and metals, polymer blends, sandstone and carbonate rocks, and cement-based materials, must be considered as random composites at the micrometer scale or lower. Their microstructures cannot be well-described by this inclusion-matrix picture. In fact, usually the only direct microstructural information one has to work with in these kinds of random materials are actual digital images. These can be 2-D images acquired using electron or light microscopy, 3-D images obtained using X-ray microtomography (Schwartz *et al.*, 1993), serial sectioning, or magnetic resonance imag-

ing, or 2-D and 3-D simulated images from digital-image-based microstructural models (Garboczi *et al.*, 1993; Pimienta *et al.*, 1992). In all these cases, any numerical algorithm developed to compute elastic properties must be able to work on an arbitrary digital image in two or three dimensions.

This paper describes such an elastic algorithm, which operates directly on digital images by treating each pixel, either a square in 2-D or a cube in 3-D, as a linear finite element. Standard finite element techniques (Cook *et al.*, 1989) are used, in combination with a conjugate gradient solver (Polak, 1971) that is able to handle the many finite elements that are necessary for adequate resolution of a microstructure. Usually periodic boundary conditions are used, but this is not necessary. Once individual phase properties are supplied, the composite material properties can be computed by applying a strain and computing the appropriate stress and/or energy averages (Hashin, 1983). Using the digital image as the finite element mesh simplifies the algorithm, since mesh generation is often the most difficult and time consuming step in using the finite element method (Cook *et al.*, 1989). This procedure also uses the maximum resolution possible from an image (one pixel equals one finite element) in the computation of elastic properties. An important feature of this algorithm is that it enables images to be made of the stress or strain fields, which can then be compared with microstructural features.

It should be emphasized that the above algorithm uses only the simplest version of the general finite element method. Higher order interpolations could be used for each pixel, improving the accuracy of the method by using quadratic or higher order interpolations for the displacement field. This would require, however, that additional nodes be assigned to each pixel, say at the middle or at the faces, because of the additional unknown coefficients in such an interpolation scheme. We believe it to be preferable, at least in a general algorithm for arbitrary complex random materials, to stay with a simple cubic lattice and use, if possible, higher resolution (more pixels per microstructural feature) with the same linear interpolation scheme to make the approximate displacement field more accurate. This type of algorithm has also been used to solve complicated 3-D intrinsic conductivity and viscosity problems (Douglas and Garboczi, 1995).

This elastic algorithm in particular, and the finite element method in general, are closely related to spring network problems. By an appropriate choice of force constants, a spring network on a square lattice with spring stretching and bending forces may be mapped exactly onto our finite element scheme for a geometrically similar 2-D array of square pixels (Day *et al.*, 1995).

We use a recently developed digital-image-based algorithm for generating the random microstructures studied in this paper (Schwartz *et al.*, 1991). The algorithm does not repeatedly embed inclusions in a matrix, but rather uses a convolution and thresholding scheme.

Consider an intensity function defined on a simple cubic lattice, $I_o(i,j,k)$. $I_o(i,j,k)$ is initially a white noise random field, with the values of I_o evenly and randomly distributed between 0 and 1. Now define a kernel function $\mathrm{Ke}(i'\text{-}i, j'\text{-}j, k'\text{-}k)$, and define a new intensity $J(i,j,k)$ via:

$$J(i,j,k) = \Sigma_{i'}\Sigma_{j'}\Sigma_{k'} \mathrm{Ke}(i'-i, j'-j, k'-k) I_0(i', j', k'). \tag{1}$$

A threshold J_c is then chosen, so that the final two-phase microstructure $I(i,j,k)$ is generated by:

$$I(i,j,k) = 1 \quad \text{if} \quad J(i,j,k) < J_c,$$
$$I(i,j,k) = 2 \quad \text{if} \quad J(i,j,k) > J_c. \tag{2}$$

Many choices of the kernel Ke are possible. A particularly simple one, that was used previously to model the pore structure of carbonate rocks (Schwartz *et al.*, 1991), is a Gaussian:

$$\text{Ke}(x,y,z) \sim \exp(-r^2/w^2), \quad r^2 = x^2+y^2+z^2. \tag{3}$$

The value of w sets the length scale of the correlations in the microstructure. The resulting microstructure, as represented by $I(i,j,k)$ and for the kernel in (3), has been shown, using different values of J_c, to give microstructures where one phase can be considered as the matrix and the other phase as inclusions, and a broad region, between about 20% volume fraction limits for each phase, where each phase forms a fully connected network (Schwartz *et al.*, 1991). In this bi-continuous region, the usual matrix-inclusion ideas used to understand composites are not necessarily useful. This is the region of most interest to us (Day and Garboczi, 1995).

Figure 1 shows a cross-section of one of these 3-D composites, at a volume fraction of 50%. The image is 128^2 pixels in size, sliced from a 128^3 system, using the kernel of (3) with $w = 5$. In 2-D, of course, only one phase percolates at a time, and the common percolation threshold for systems generated with the 2-D version of this kernel is at 50% area fraction, which agrees with a previous analysis of similar

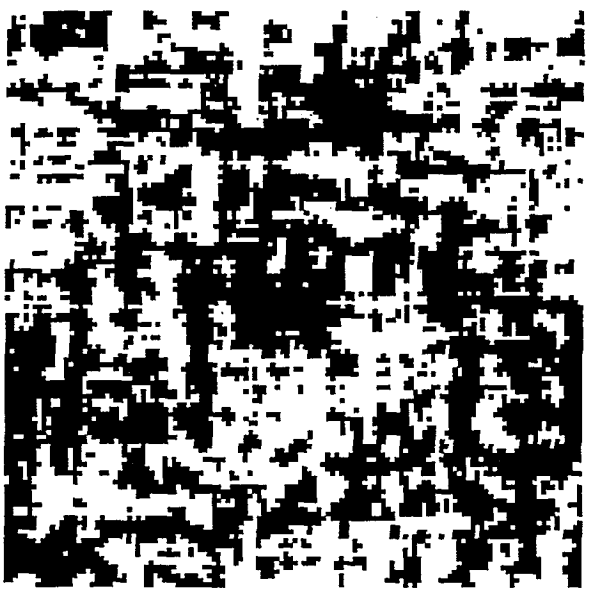

Fig. 1. Showing a 128×128 slice through a 128^3 Gaussian kernel-based microstructure ($w = 5$, $c_1 = c_2 = 0.50$).

microstructures (Zallen and Scher, 1971). In the limit of infinite resolution, $I(i,j,k) \rightarrow I(x,y,z)$, a smooth function (Blumenfeld and Torquato, 1993).

3. EFFECTIVE MEDIUM THEORY

There are many ways to develop effective medium theories (EMTs) that attempt to predict the effective elastic properties of a composite (Hashin, 1983; Torquato, 1991). The usual approach is to exactly solve a one-inclusion problem, in the dilute limit, and then use some sort of averaging process to generate a formula that predicts effective properties at general volume fractions. We use a 2-D EMT for elliptical inclusions (Thorpe and Sen, 1985), a 3-D EMT developed for spherical inclusions (Budiansky, 1965), and a 3-D EMT developed for inclusions shaped like ellipsoids of revolution (Berryman, 1980). We will also discuss the equivalent EMT for hyperspherical inclusions in d dimensions.

The 2-D EMT has been previously discussed (Snyder *et al.*, 1992; Day *et al.*, 1992). The equations for the 3-D EMT in the case of spherical inclusions can be derived (Budiansky, 1965) by requiring that for a composite subjected to a uniform external shear stress τ^0, the average shear strain $\bar{\gamma}$ for the composite is just

$$\bar{\gamma} = \frac{\tau_0}{G} = c_1\bar{\gamma}_1 + c_2\bar{\gamma}_2, \tag{4}$$

$$\bar{\gamma}_i = \frac{\tau_0}{G+\beta(G_i-G)} \tag{5}$$

where γ_i is the average strain in the ith phase, G is a shear modulus, and where

$$\beta = \frac{2(4-5\nu)}{15(1-\nu)} \tag{6}$$

which depends only on the (as yet unknown) effective Poisson ratio of the composite. In (4)–(6) the subscripts refer to the phase label, unsubscripted variables are the unknown effective quantities, and c_i is the volume fraction of the ith phase. A similar calculation for the bulk modulus leads to the coupled equations for the effective moduli

$$\frac{1}{G} = \frac{c_1}{G+\beta(G_1-G)} + \frac{c_2}{G+\beta(G_2-G)} \tag{7}$$

$$\frac{1}{K} = \frac{c_1}{K+\alpha(K_1-K)} + \frac{c_2}{K+\alpha(K_2-K)}, \tag{8}$$

where

$$\alpha = \frac{(1+\nu)}{3(1-\nu)} \tag{9}$$

depends only on the (unknown) Poisson's ratio of the composite.

As has been pointed out (Budiansky, 1965), when $\alpha = \beta$ the bulk and shear moduli

have the same functional form and so the Poisson ratio remains constant for any values of c_i. This occurs in 3-D for $\nu_1 = \nu_2 = \nu^* = 1/5$. The value $\nu^* = 1/5$ is also the EMT prediction for the fixed point to which the Poisson's ratio is drawn, for any starting value of Poisson's ratio, when one phase has zero moduli and a zero-modulus percolation threshold is approached (Day *et al.*, 1992). The formulas for ellipsoidal inclusions are much more complicated, and are given in detail elsewhere (Berryman, 1980).

The d-dimensional EMT that is based on hyperspherical inclusions has previously been presented for the case where one phase has zero moduli, though without any details (Bergman and Kantor, 1984†). The general form of the equations is the same as (7) and (8) except α and β will be different, depending on the dimension d. If we make the assumption that in general α and β will only depend on the effective Poisson's ratio of the composite, as was the case both in 2-D and in 3-D, the general forms can be extracted from the zero moduli result (Bergman and Kantor, 1984):

$$\alpha = \frac{(1+\nu)}{d[1+\nu(2-d)]}, \tag{10}$$

$$\beta = \frac{2[\nu(d^2-d-1)-(d-1)]}{d(d+2)[\nu(d-2)-1]}. \tag{11}$$

Once again, (7) and (8) give the same functional form for G and K when $\alpha = \beta$, or when $\nu = 1/(2d\text{-}1)$, which is then a fixed point of the effective medium theory, for any stiffness ratio E_1/E_2. The value $\nu^* = 1/(2d\text{-}1)$ is the EMT prediction for the fixed point to which the Poisson's ratio is drawn, for any starting value of Poisson's ratio, when one phase has zero moduli and a zero-modulus percolation threshold is approached (Bergman and Kantor, 1984). Bergman *et al* have presented this result in terms of the ratio $(K/G)^* = 4/d$. This is seen to be equivalent by substitution into the expression for the d-dimensional Poisson's ratio:

$$\nu = \frac{dK-2G}{d(d-1)K+2G} \tag{12}$$

4. TESTS OF ELASTIC ALGORITHM

The algorithm described above has been developed specifically to be applied to images of random materials that have been generated either using a microstructure model, or by an experimental technique like X-ray tomography. Especially in the latter case, it is usually difficult to perform checks such as how the results depend on the size of the image or on the resolution of the image. However, such checks can easily be done with model systems, especially ones which have an analytically known solution, to give an idea of what the error might be in any given computation using real images.

There are several sources of error in using this algorithm on a specific random

† There are serious misprints in (14) of this paper. We thank M. F. Thorpe for providing us with the correct form of the equations for voids.

Table 1. *Finite size scaling effect on* w = 5 *2-D results*

System size	Young's modulus	Poisson's ratio
32	2.408±0.488	0.384±0.092
64	2.627±0.227	0.341±0.028
128	2.673±0.205	0.320±0.039
256	2.633±0.066	0.325±0.012
512	2.624±0.059	0.326±0.013

Table 2. *Dilute limit for circle—effect of digital resolution*

System size	M_K	% diff.	M_G	% diff.
20	1.548	10.1	1.318	6.9
40	1.548	10.1	1.362	12.9
80	1.475	4.9	1.290	4.6
160	1.447	2.9	1.261	2.3
320	1.433	1.9	1.251	1.5
640	1.425	1.3	1.244	0.9

system. The first is finite size error—does the image contain enough of the random structure so that the computed elastic moduli no longer depend on system size? The second error is: how much do different realizations of the same size random system differ from each other? The third source of error is: how does the resolution of microstructural features affect the results? A fourth source of error, how well the minimum energy state is approximated in the solution algorithm, is much smaller, essentially on the order of the round-off error of the computer, and so is negligible except in cases where there is a large contrast in the stiffness of the two phases. Several series of runs were made to estimate these sources of error.

Table 1 shows the effect of system size, at a fixed resolution, on the computed elastic moduli. The simulations are for a fixed value of $w = 5$ for a 2-D Gaussian system, averaged over 10 samples. The area fraction of phases 1 and 2 were fixed at 0.5 each ($E_1/E_2 = 10$, $\nu_1 = \nu_2 = \frac{1}{3}$). The average values of E and ν change little for system size greater than 64. The standard deviation over the average of 10 independent systems decreases as the system size increases.

Table 2 shows the effect of resolution on the computed dilute limit slopes for circles embedded in a matrix, for the same choice of moduli as in Table I (the circle is the stiffer phase). The slopes are defined by

$$\frac{K}{K_m} = 1 + M_K c, \tag{13}$$

$$\frac{G}{G_m} = 1 + M_G c, \tag{14}$$

where m is for matrix and i is for inclusion and c is the area fraction of the inclusion.

Table 3. *2-D elastic checkerboard—equal shear moduli case*

System size	K	% diff.	E	% diff.	ν	% diff.
2	5.500	96.4	5.866	25.7	0.4667	180
4	3.271	16.8	4.964	6.4	0.2411	44.7
8	2.937	4.9	4.759	2.0	0.1897	13.8
16	2.841	1.5	4.695	0.6	0.1737	4.2
32	2.812	0.4	4.675	0.2	0.1688	1.3
64	2.804	0.1	4.669	0.05	0.1673	0.4
128	2.8012	0.04	4.6675	0.02	0.16687	0.1
256	2.8003	0.01	4.6669	0.005	0.16672	0.03
512	2.8001	0.004	4.6667	0.0007	0.16668	0.008

The slopes M are a function of the geometry of the inclusion and of the relative values of the four moduli (Thorpe and Sen, 1985). Each data point is for a circle whose diameter is one tenth the size of the periodic unit cell, so that there is little or no influence from the periodic boundary conditions. Increasing the system size in terms of the number of pixels per unit length also improves the resolution of the circle. Table 2 shows that a circle diameter of 16 pixels is sufficient to bring the computed initial slope within 3% of the theoretical value.

Table 3 shows results for a 2-D regular elastic checkerboard, where the unit cell contained four "checks" (two black, two white), so that the size of each check was one half the system size. By making the shear moduli equal, exact results can be obtained for all the effective moduli that are independent of microstructure ($G_1 = G_2 = 2$, $K_1/K_2 = 10$). In 2-D, the exact Young's modulus E and Poisson's ratio ν for this case are (Thorpe and Jasiuk, 1994):

$$E = c_1 E_1 + c_2 E_2, \tag{15}$$

$$\nu = c_1 \nu_1 + c_2 \nu_2. \tag{16}$$

Table 3 shows that by a system size where the check size is only 8 × 8 pixels, the error in K and E is less than one percent. The error in ν is always a bit bigger, as it is a ratio between two uncertain quantities.

Table 4 shows results similar to that of Table 3, but for the 2-D Gaussian system. The ratio of w to the system size is fixed, and the system size is changed, so that the resolution of individual features increases with system size. Here the same values for

Table 4. *Resolution scaling for 2-D Gausian system*

System size (w)	K	% diff.	E	% diff.	ν	% diff.
32 (1.25)	2.941	5.0	4.762	2.0	0.1905	14.3
64 (2.5)	2.864	2.3	4.711	1.0	0.1777	6.6
128 (5)	2.830	1.1	4.688	0.5	0.1719	3.1
256 (10)	2.828	1.0	4.686	0.4	0.1715	2.9
512 (20)	2.824	0.9	4.683	0.3	0.1708	2.5

the individual phase moduli are used as in Table 3, so that the exact values for the effective moduli are also the same. If we consider that the size of the individual features in the microstructure of these Gaussian images are on the order of w, the correlation length, then the Gaussian systems obtain the same sort of accuracy in E and ν as does the checkerboard when comparing w to the size of one check. Having many more digitally rough interfaces in the Gaussian system does not cause the accuracy to significantly degrade compared to the checkerboard.

In 3-D, where simulations are much more computer-time intensive, one test was run for a 64^3, $w = 5$ Gaussian system with $G_1 = G_2 = 2$, and $K_1/K_2 = 10$, the same numerical values as were used in 2-D. The exact values for the moduli were (Hill, 1963): $K = 3.02041$, $E = 4.91513$, and $\nu = 0.228782$. The numerical results were all within 2% of these exact values, implying that the resolution was adequate and similar to that found in 2-D.

5. NUMERICAL RESULTS

The error tests of the previous section show that the system sizes and resolutions that were chosen to be used to compute the main results, 128^2 ($w = 5$) in 2-D and 64^3 ($w = 5$) in 3-D, averaged over five independent realizations, were adequate to give roughly 5% accuracy in the results now presented.

A series of five realizations of microstructures were created using a Gaussian kernel for a range of concentrations c_1 and c_2. The ratio of E_1/E_2 was held fixed at 10, and a range of Poisson's ratios $\nu_1 = \nu_2 = \nu_0$ was investigated. Figure 2 shows the 3-D results for the composite Poisson's ratio, averaged over the five realizations, as a

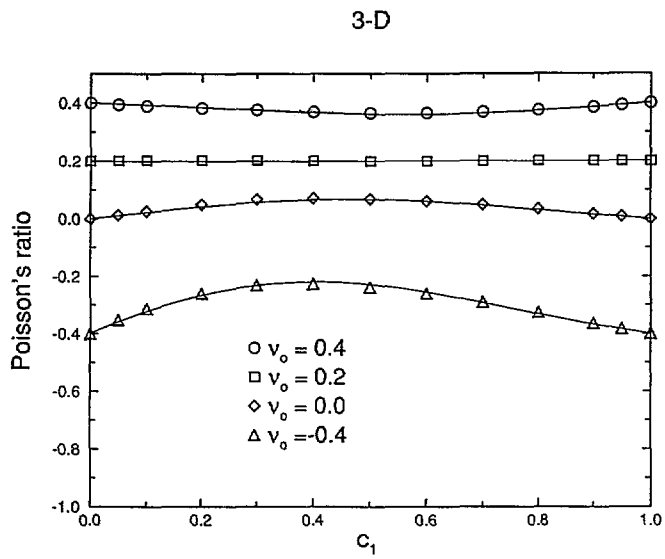

Fig. 2. Showing the 3-D effective Poisson's ratios vs phase fraction for a stiffness ratio of 10. The lines are the graphs of the EMT equations (4)–(7), and the symbols are numerical results for the 3-D Gaussian kernel-based microstructure.

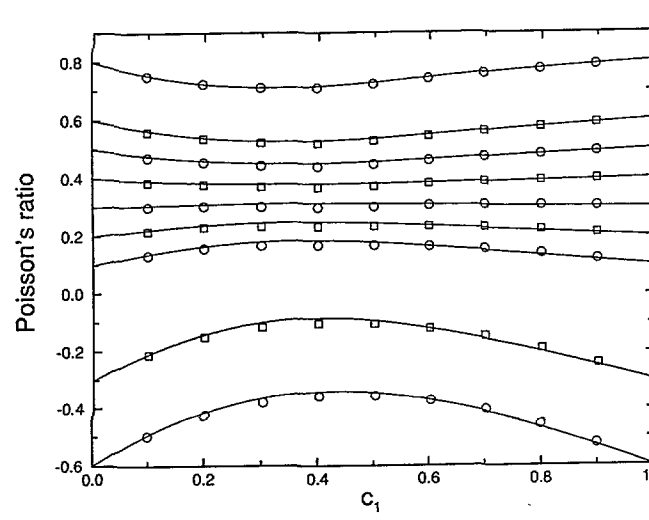

Fig. 3. Showing the 2-D effective Poisson's ratios vs phase fraction for a stiffness ratio of 10. The lines are the graphs of the 2-D EMT equations (Thorpe and Sen, 1985), and the symbols are numerical results for the 2-D Gaussian kernel-based microstructure.

function of c_1. The system size was 64^3, and $w = 5$ in the Gaussian kernel of (3). The solid lines are the EMT predictions of (4)–(7). The EMT results describe the numerical results well. The numerical results are in agreement with the EMT predictions for the behavior of the effective Poisson's ratio ν, in that when $\nu_1 = \nu_2 = 1/5$, $\nu = 1/5$ as well for all volume fractions. Also, when $\nu_1 = \nu_2 > 1/5$, $1/5 < \nu < \nu_1 = \nu_2$, and when $\nu_1 = \nu_2 < 1/5$, $\nu_1 = \nu_2 < \nu < 1/5$. This result is also predicted by a "differential method" EMT (Zimmerman, 1995). The EMT also accurately fits the Young's modulus results, which are shown elsewhere (Day *et al.*, 1995). We have also checked that the minimum value for ν, when $\nu_1 = \nu_2 > 1/5$, and the maximum value for ν, when $\nu_1 = \nu_2 < 1/5$, depend on the stiffness contrast between the two phases. These extremum values approach 1/5 as the stiffness contrast diverges, as can be seen by solving the EMT equations.

We have carried out the equivalent simulations in 2-D, for values of Poisson's ratio *that were not accessible to our previous algorithm, and have confirmed* the EMT results found before (Snyder *et al.*, 1992). Results are displayed in Fig. 3.

6. DISCUSSION AND CONCLUSIONS

The result found is that when $\nu_1 = \nu_2$, there is a critical value of Poisson's ratio, ν^*, that separates the ν vs volume fraction graph into two distinct regions. Below ν^*, the effective Poisson's ratio ν is such that $\nu_1 = \nu_2 < \nu < \nu^*$, and above ν^*, $\nu_1 = \nu_2 > \nu > \nu^*$.

This result was true for d-dimensional EMTs based on spherical inclusions, and for the quite general Gaussian kernel-based microstructure in 2-D and 3-D. The question may be raised: is this behavior independent of microstructure, at least for isotropic systems, or is it dependent on the spherical inclusion microstructure? The Gaussian kernel-based microstructure is not based on spherical inclusions, but in the small c_1 or c_2 limit, when either phase is discontinuous, the inclusions that result should be roughly spherical, since the kernel in (3) is isotropic. We have checked this limit visually, by generating images, and by computing K and G in these limits. The asymptotic slopes for the effective values of K and G agree fairly well with the exact result for spherical particles (Budiansky, 1965). Visually examining the microstructural images in this limit also reveals that there is indeed a rough sphericity present in the isolated particles of the dilute phase. This may be the reason why the sphere-based EMT seems to work so well.

One way to check for the behavior of the effective Poisson's ratio in other microstructures is by using a 3-D EMT for inclusions shaped like ellipsoids of revolution (Berryman, 1980), and studying its predictions for highly non-spherical shapes. Judging by the good agreement between simulation and EMT in Fig. 2, we expect that a similarly-derived EMT for ellipsoids of revolution should be reasonably trustworthy, at least as long as there is not too much of an elastic contrast between phases, and so do not carry out the numerical computations. These computations would, however, be possible for our algorithm. The only problem would be the lack of resolution in 3-D, because of computer memory limitations, to adequately represent a sufficient number of ellipsoids to get good statistics for the random geometry.

Figure 4(a) shows the effective Poisson's ratio vs volume fraction for prolate inclusions with an aspect ratio of 20, which is a very elongated ellipsoid, and a stiffness ratio of 10 (inclusion to matrix). The same picture is preserved as in Figs 2 and 3. Figure 4(b) shows a vertically expanded view of the same results, showing the S-shaped behavior around $\nu_1 = \nu_2 = 1/5$. This behavior persists from about $\nu_1 = \nu_2 = 0.18$ to about $\nu_1 = \nu_2 = 0.23$. Outside this region, no significant qualitative difference is seen from the previous EMT and numerical results. The EMT results for oblate ellipsoids are similar, with similar behavior for ellipses found in 2-D (Snyder *et al.*, 1992).

We therefore tentatively suggest that the behavior of the Poisson's ratio, when the two-phase Poisson's ratios of the composite are equal, is generic. To a good approximation, this behavior does not depend on microstructure, with the critical value $\nu_1 = \nu_2 = \nu^* = 1/(2d-1)$ in d dimensions. We expect that generally, when $\nu_1 = \nu_2 > \nu^*$, the value of the effective Poisson's ratio will decrease as the two phases are mixed, with a minimum value, dependent on the stiffness contrast between the two phases (Snyder *et al.*, 1992), that is bounded below by $\nu_1 = \nu_2$. When $\nu_1 = \nu_2 < \nu^*$, the value of the effective Poisson's ratio will increase as the two phases are mixed, with a maximum value that does not exceed $\nu_1 = \nu_2$ and that also depends on the elastic stiffness contrast between the two phases.

Finally, the elastic algorithm presented in this paper has shown itself to be a straightforward and accurate way of computing the linear elastic properties of heterogeneous materials. The only limitation of the algorithm is if the maximum size digital image that can be handled by a given computer is large enough to adequately represent the microstructure of interest, and give moduli results of a desired accuracy.

(a)

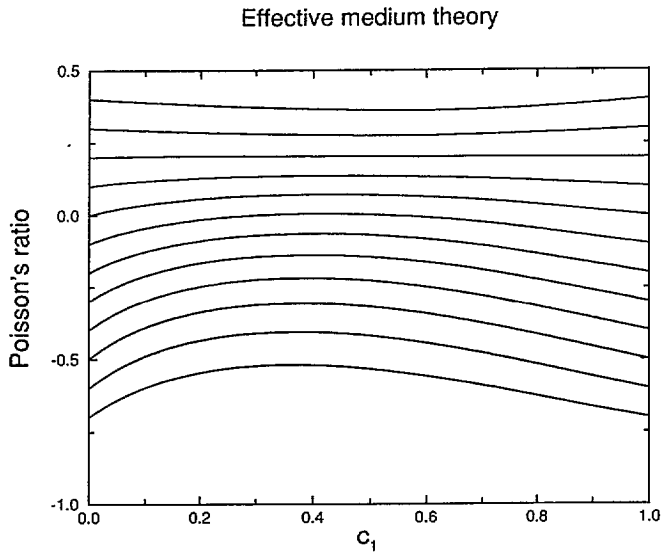

(b)

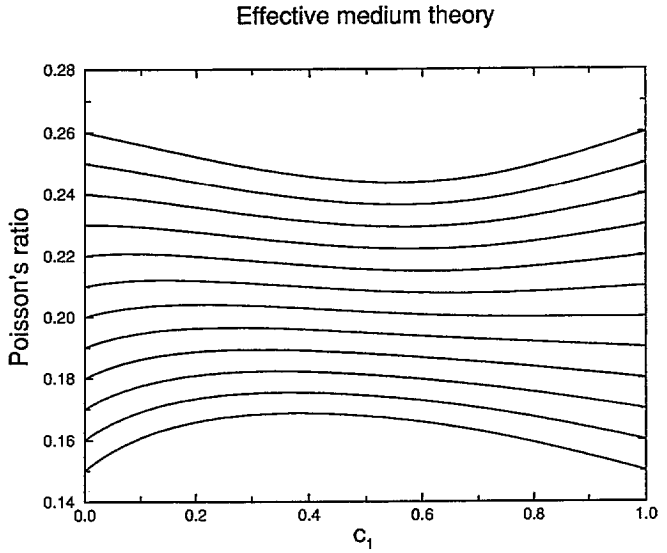

Fig. 4. Showing the 3-D effective Poisson's ratios vs phase fraction for a stiffness ratio of 10, for prolate ellipsoidal inclusions with an aspect ratio of 20. The lines are the graphs of the full 3-D EMT equations (Berryman, 1980): (a) Full scale; (b) vertical expanded scale showing region around $v^* = 1/5$

Future work includes using this elastic algorithm to simulate cases where applied stresses can affect the actual growth of a microstructure (Bullard *et al.*, 1995), and to analyze the elastic properties of a given microstructure.

ACKNOWLEDGMENTS

We would like to acknowledge useful discussions with M. F. Thorpe, E. R. Fuller, W. C. Carter, A. Jagota and S. Torquato. ARD would like to acknowledge partial financial support from NIST for some of the work described in this paper.

REFERENCES

Bergman, D. J. and Kantor, Y. (1984) Critical properties of an elastic fractal. *Phys. Rev. Letts.* **53**, 511–514.

Berryman, J. G. (1980) Long-wavelength propagation in composite elastic media II. Ellipsoidal inclusions. *J. Acoust. Soc. Am.* **68**, 1820–1831.

Blumenfeld, R. and Torquato, S. (1993) Coarse-graining procedure to generate and analyze heterogeneous materials: Theory. *Phys. Rev. E* **48**, 4492–4500.

Budiansky, B. (1965) On the elastic moduli of some heterogeneous materials. *J. Mech. Phys. Solids* **13**, 223–227.

Bullard, J. W., Garboczi, E. J., Carter, W. C. and Fuller, E. R. (1995) Effect of applied stresses on void growth during sintering. Unpublished.

Cook, R. D., Malkus, D. S. and Plesha, M. E. (1989) *Concepts and Applications of Finite Element Analysis*. Wiley, New York.

Day, A. R. and Garboczi, E. J. (1995) Elastic moduli and electrical conductivity of a model interpenetrating-phase composite. To be submitted to *J. Am. Ceram. Soc.*

Day, A. R., Snyder, K. A., Garboczi, E. J. and Thorpe, M. F. (1992) Elastic moduli of a sheet containing circular holes. *J. Mech. Phys. Solids* **40**, 1031–1051.

Day, A. R., Jha, P. and Yang, Y. (1996) Elastic moduli of a two-dimensional isotropic elastic sheet with elliptical holes: Computer simulations and effective medium theory. To be submitted to *J. Mech. Phys. Solids*.

Douglas, J. F. and Garboczi, E. J. (1995) Intrinsic viscosity and the polarizability of particles having a wide range of shapes. *Adv. Chem. Phys.* (in press).

Garboczi, E. J. and Bentz, D. P. (1993) Computational materials science of cement-based materials. *Mat. Res. Soc. Bull.* **18**, 50–54.

Hashin, Z. (1983) Analysis of composite materials: A survey. *J. Appl. Mech.* **50**, 481–505.

Hill, R. (1963) Elastic properties of reinforced solids: Some theoretical principles. *J. Mech. Phys. Solids* **11**, 357–372.

Pimienta, P., Carter, W. C. and Garboczi, E. J. (1992) Cellular automaton algorithm for surface mass transport due to curvature gradients: Simulations of sintering. *Comp. Mater. Sci.* **1**, 63–77.

Polak, E. (1971) *Computational Methods in Optimization*. Academic Press, New York.

Schwartz, L. M., Crossley, P. A. and Banavar, J. R. (1991) Image-based models of porous media: Application to Vycor glass and carbonate rocks. *Appl. Phys. Lett.* **59**. 3553–3555.

Schwartz, L. M., Auzerais, F., Dunsmuir, J., Martys, N. S., Bentz, D. P. and Torquato, S. (1993) Transport and diffusion in three dimensional composite media. *Physica A* **207**, 28–36.

Snyder, K. A., Garboczi, E. J. and Day, A. R. (1992) The elastic moduli of simple two-dimensional isotropic composites: Computer simulation and effective medium theory. *J. Appl. Phys.* **72**, 5948–5955.

Thorpe, M. F. and Jasiuk, I. (1994) New results in the theory of elasticity for two-dimensional composites. *Proc. Roy. Soc. Lond. A* **438**, 531–544.

Thorpe, M. F. and Sen, P. N. (1985) Elastic moduli of two dimensional composite continua with elliptical inclusions. *J. Acoust. Soc. Am.* **77**, 1674.

Torquato, S. (1991) Random heterogeneous media: Microstructure and improved bounds on effective properties. *Appl. Mech. Rev.* **44**, 37–76.

Watt, J. P., Davies, G. F. and O'Connell, R. J. (1976) The elastic properties of composite materials. *Rev. Geophys. Space Phys.* **14**, 541–563.

Zallen, R. and Scher, H. (1971) Percolation on a continuum and the localization–delocalization transition in amorphous semiconductors. *Phys. Rev. B* **4**, 4471–4478.

Zimmerman, R. W. (1995) Behavior of the Poisson ratio of a two-phase composite material in the high-concentration limit. *Appl. Mech. Rev.* (in press).